

Shortening the runtime using larger time steps for the simulation of marine ecosystem models

Markus Pfeil¹ and Thomas Slawig¹

¹Kiel Marine Science – Centre for Interdisciplinary Marine Science, Dep. of Computer Science, Kiel University, 24098 Kiel, Germany

Correspondence: Markus Pfeil (mpf@informatik.uni-kiel.de)

Abstract. The reduction of computational costs for marine ecosystem models is important for the investigation and detection of the relevant biogeochemical processes because such models are computationally expensive. In order to lower these computational costs by means of larger time steps we investigated the accuracy of steady annual cycles (i.e., an annual periodic solution) calculated with different time steps. We compared the accuracy for a hierarchy of biogeochemical models showing an increasing complexity and computed the steady annual cycles with offline simulations that are based on the transport matrix approach. For each of these biogeochemical models, we obtained practically the same solution even though larger time steps. This indicates that larger time steps shortened the runtime with an acceptable loss of accuracy.

1 Introduction

Shortening the runtime for simulations of marine ecosystem models is important for computing steady annual cycles. In general, marine ecosystem models are an essential element to investigate the influence of various biogeochemical processes in the marine carbon cycle. The ocean biota, for example, processes different climatically relevant chemical elements and the ocean takes up carbon from the atmosphere and stores it. Due to the interplay of physical and biogeochemical processes, a marine ecosystem model consists of a global ocean circulation model coupled to a biogeochemical model (cf. Fasham, 2003; Sarmiento and Gruber, 2006). While the equations and variables of the physical processes are well known, a set of state variables or equations describing the biogeochemical processes is generally not available. Therefore, there is a wide range of biogeochemical models which differ in their complexity due to the number of state variables and parameterizations (see e.g., Kriest et al., 2010; Keller et al., 2012; Ilyina et al., 2013; Yool et al., 2013; Le Quéré et al., 2016). The validation of these models requires many calculations of steady annual cycles. More specifically, the validation, which contains a parameter estimation and a discussion of simulation results, assesses the steady annual cycles against given observational data (Fennel et al., 2001).

The computational effort is tremendous for any fully coupled simulation because a single model evaluation is already computationally expensive (Oschlies, 2006). This results from the simultaneous computation of the ocean circulation and the biogeochemical model in three spatial dimensions. In particular, the computational cost increases for the computation of a steady annual cycle due to the necessary long-time integration (cf. Bernsen et al., 2008). In typical cases, the simulation needs

at least several thousand model years to reach a steady annual cycle (cf. Bryan, 1984; Danabasoglu et al., 1996; Bernsen et al., 2008).

Several strategies address the reduction of the computational costs in order to compute a steady annual cycle in marine ecosystem models (e.g. Bryan, 1984; Danabasoglu et al., 1996; Wang, 2001; Siewertsen et al., 2013). Firstly, spatial parallelization using domain decomposition methods lowers the computational costs. Instead of using the fully coupled simulation (the so-called *online* simulation), the *offline* simulation, secondly, neglects the influence of the biogeochemical model on the ocean circulation and, hence, applies a pre-computed ocean circulation. A third strategy is the use of Newton's method instead of the long-time integration. Lastly, the application of graphics processing units shortens the computational time. This constitutes only an excerpt of the strategies for the reduction of the computational costs.

Khatiwala et al. (2005) reduced the computational effort with a tolerable loss of accuracy by implementing the transport matrix method (TMM) as offline simulation, which approximated the general ocean circulation by pre-computed transport matrices. On the one hand, this reduced the computation of the ocean circulation to matrix-vector multiplications and, on the other hand, separated the evaluation of the biogeochemical model from the ocean circulation neglecting the very small effects of biogeochemical tracers on the density (e.g., via solar heating) (Oschlies, 2004). Khatiwala (2007) showed that the accuracy of this method using the linearized tracer transport is sufficient for marine ecosystem models to obtain first insights on a global basin scale. The method also provides the flexibility to replace the long-time integration with Newton's method (Khatiwala, 2008).

The computational time to compute a steady annual cycle strongly affects the computational effort of a parameter optimization or sensitivity study, since several hundred computations of steady annual cycles are necessary. With the help of parameter optimization of global biogeochemical models, the optimal model parameters are determined so that the model ideally reflects the real-world data (Kwon and Primeau, 2006, 2008; Prieß et al., 2013). This is especially necessary to optimize the poorly known model parameters.

In order to lower the computational costs, we have investigated, in this paper, the influence of larger time steps on the accuracy of the computation of steady annual cycles for both the biogeochemical model (Dutkiewicz et al., 2005) which is part of the MITgcm ocean model and a hierarchy of biogeochemical models with an increasing complexity (Kriest et al., 2010). To our knowledge, there is no systematic investigation of this influence in the literature. However, this is essential for the selection of an appropriate time step to lower the computational effort of those computations. Indeed, some studies had already used larger time steps (e.g., Prieß et al., 2013; Kriest et al., 2017) and, in particular, the use of larger time steps shortened the runtime with an acceptable loss of accuracy.

This paper is organized as follows: after an introduction to the general structure of marine ecosystem models, we describe in Sect. 2 the TMM and the computation of a steady annual cycle. In Sect. 3, we present the computation using larger time steps. Section 4 covers numerical results in which different time steps were used. The paper closes with conclusions deduced from the numerical results in Sect. 5.

2 Model description

A marine ecosystem model usually consists of a component describing the ocean circulation and a component representing the biogeochemical model (e.g., Fasham, 2003; Fennel and Neumann, 2004; Sarmiento and Gruber, 2006). Biogeochemical tracers are substances in the ocean water that are subject to chemical or biochemical reactions. The equations modeling the ocean circulation including temperature and salinity distribution are coupled to equations regulating the transport and the reactions of the biogeochemical tracers. The couplings are based on the fact that the ocean circulation affects the tracer concentrations and the turbulent mixing of marine water dominates the diffusion of the tracer concentrations and, vice versa, the tracer concentrations influence the ocean circulation. However, a fully coupled simulation (also called *online* model) in three spatial dimensions is limited to single model evaluations, even on high performance computing clusters, because the simulation of both systems must be carried out simultaneously and the computational effort, therefore, is enormous.

Instead of the online model, the *offline* model simplifies the simulation. The offline simulation uses passive tracers which do not have an effect on the ocean physics or neglects this impact. Consequently, the coupling is only a one-way coupling from the ocean circulation to the tracer dynamics. Due to the one-way coupling for offline simulations, we can apply a pre-computed ocean circulation. We applied offline models with an increasing complexity of the biogeochemical models as marine ecosystem models, thus they were introduced by Krist et al. (2010); Dutkiewicz et al. (2005).

2.1 Model equations for marine ecosystems

A system of differential equations describes the marine ecosystem model. The differential equations are of the Lotka-Volterra or predator-prey type, and the number of tracers defines the size of the system of differential equations (Lotka, 1910; Volterra, 1931). We consider, in the rest of this paper, marine ecosystem models using an offline model with $n_y \in \mathbb{N}$ tracers on a spatial domain $\Omega \subset \mathbb{R}^3$ (i.e., the ocean) and on a time interval $[0, 1]$ (i.e., one model year). For $i \in \{1, \dots, n_y\}$, $y_i : \Omega \times [0, 1] \rightarrow \mathbb{R}$ denotes the function of the tracer concentration and $\mathbf{y} := (y_i)_{i=1}^{n_y}$ the vector of all tracers. The following system of parabolic partial differential equations describes the tracer transport of a marine ecosystem model

$$\frac{\partial y_i}{\partial t}(x, t) + (D(x, t) + A(x, t))y_i(x, t) = q_i(x, t, \mathbf{y}, \mathbf{u}), \quad x \in \Omega, t \in [0, 1], \quad (1)$$

$$\frac{\partial y_i}{\partial n}(x, t) = 0, \quad x \in \partial\Omega, t \in [0, 1], \quad (2)$$

for $i = 1, \dots, n_y$, including linear operators $D : \Omega \times [0, 1] \rightarrow \mathbb{R}$ and $A : \Omega \times [0, 1] \rightarrow \mathbb{R}$, which corresponds to the diffusion and advection coming from the ocean circulation, and the term $q_i : \Omega \times [0, 1] \rightarrow \mathbb{R}$, $(x, t) \mapsto q_i(x, t, \mathbf{y}, \mathbf{u})$ for the tracer y_i of the biogeochemical model. The Neumann boundary conditions (2) which include the normal derivative are appropriate boundary conditions on $\partial\Omega$ for all tracers. Instead of the inhomogeneous Neumann boundary conditions taking the flux interactions, for example, with the atmosphere or sediment into account, we apply the homogeneous Neumann boundary conditions without tracer fluxes on the boundary.

Both the advection and the diffusion determine the tracer transport in marine water. With a given velocity field $v : \Omega \times [0, 1] \rightarrow \mathbb{R}^3$, the advection is defined as

$$A(x, t)y_i(x, t) := \operatorname{div}(v(x, t)y_i(x, t)), \quad x \in \Omega, t \in [0, 1] \quad (3)$$

for $i \in \{1, \dots, n_y\}$. In ocean circulation modeling, the horizontal and vertical direction of the diffusion are usually considered separately because of the quite different spatial scales requiring an implicit treatment of the vertical part in time integration. Thus, the diffusion operator $D = D_h + D_v$ consists of a horizontal and a vertical part defined by

$$D_h(x, t)y_i(x, t) := -\operatorname{div}_h(\kappa_h(x, t)\nabla_h y_i(x, t)) \quad x \in \Omega, t \in [0, 1], \quad (4)$$

$$D_v(x, t)y_i(x, t) := -\frac{\partial}{\partial z} \left(\kappa_v(x, t) \frac{\partial y_i}{\partial z}(x, t) \right), \quad x \in \Omega, t \in [0, 1] \quad (5)$$

for $i \in \{1, \dots, n_y\}$, where div_h and ∇_h denote the horizontal divergence and gradient, $\kappa_h, \kappa_v : \Omega \times [0, 1] \rightarrow \mathbb{R}$ the diffusion coefficient fields and z the vertical coordinate. The diffusion coefficient fields κ_h, κ_v and, therefore, the tracer transport are identical for all tracers if the molecular diffusion of the tracers is considered to be negligible compared to the turbulent mixing, which is a suitable simplification.

The biogeochemical model includes the biogeochemical processes within the ecosystem. In contrast to the biogeochemical model, the marine ecosystem model additionally contains the effects of the ocean circulation and, thus, represents the whole system (1) to (6). For $i \in \{1, \dots, n_y\}$, the generally nonlinear function $q_i : \Omega \times [0, 1] \rightarrow \mathbb{R}, (x, t) \mapsto q_i(x, t, \mathbf{y}, \mathbf{u})$ describes the biogeochemical processes including the coupling to the other tracers for the tracer y_i . These functions q_i depend firstly on space and time due to the variability of the solar radiation and its influence on the biogeochemical processes, secondly on the different tracers and thirdly on $n_u \in \mathbb{N}$ model parameters (for example growth, loss and mortality rates or sinking speeds) summarized in a parameter vector $\mathbf{u} \in \mathbb{R}^{n_u}$. Altogether, these functions form the biogeochemical model $\mathbf{q} = (q_i)_{i=1}^{n_y}$.

For the marine ecosystem model, our aim is the calculation of a steady annual cycle, i.e., a periodic solution of (1) and (2), which additionally satisfies

$$y_i(x, 0) = y_i(x, 1), \quad x \in \Omega, \quad (6)$$

for $i \in \{1, \dots, n_y\}$. For this purpose, we assume that the operators D, A and the functions q_i are annually periodic in time.

2.2 Biogeochemical models

We applied a hierarchy of global biogeochemical models with an increasing complexity introduced by Kriest et al. (2010). Kriest et al. (2012) and Piwonski and Slawig (2016a) already applied these biogeochemical models for diverse experiments. In the following, we provide a short description of each model following the notation by Piwonski and Slawig (2016a) and refer to Kriest et al. (2010) and Piwonski and Slawig (2016a) for a detailed description of the modeled processes and model equations of each biogeochemical model in this hierarchy and, in particular, to Piwonski and Slawig (2016a, Appendix B) for the equations of the different tracers. Table 1 summarizes the model parameters for the different models of the hierarchy.

Table 1. Parameter values for the model hierarchy (\mathbf{u}_{ref}) as well as lower (\mathbf{b}_ℓ) and upper (\mathbf{b}_u) bounds for the parameter values used to generate the Latin hypercube sample for the whole model hierarchy.

Parameter	Description	\mathbf{u}_{ref}	\mathbf{b}_ℓ	\mathbf{b}_u	Unit
k_w	Attenuation coefficient of water	0.02	0.01	0.05	m^{-1}
k_c	Attenuation coefficient of phytoplankton	0.48	0.24	0.72	$(\text{mmol P m}^{-3})^{-1}\text{m}^{-1}$
μ_P	Maximum growth rate	2.0	1.0	4.0	d^{-1}
μ_Z	Maximum grazing rate	2.0	1.0	4.0	d^{-1}
K_N	Half saturation constant for PO_4 uptake	0.5	0.25	1.0	mmol P m^{-3}
K_P	Half saturation constant for grazing	0.088	0.044	0.176	mmol P m^{-3}
K_I	Light intensity compensation	30.0	15.0	60.0	W m^{-2}
σ_Z	Fraction of production remaining in zooplankton	0.75	0.05	0.95	1
σ_{DOP}	Fraction of phytoplankton and zooplankton losses assigned to DOP	0.67	0.05	0.95	1
λ_P	Linear phytoplankton loss rate	0.04	0.02	0.08	d^{-1}
κ_P	Quadratic phytoplankton loss rate	4.0	2.0	6.0	$(\text{mmol P m}^{-3})^{-1}\text{d}^{-1}$
λ_Z	Linear zooplankton loss rate	0.03	0.015	0.045	d^{-1}
κ_Z	Quadratic zooplankton loss rate	3.2	1.6	4.8	$(\text{mmol P m}^{-3})^{-1}\text{d}^{-1}$
λ'_P	Phytoplankton mortality rate	0.01	0.005	0.015	d^{-1}
λ'_Z	Zooplankton mortality rate	0.01	0.005	0.015	d^{-1}
λ'_D	Degradation rate	0.05	0.025	0.1	d^{-1}
λ'_{DOP}	Decay rate	0.5	0.25	1.0	yr^{-1}
b	Implicit representation of sinking speed	0.858	0.7	1.5	1
a_D	Increase of sinking speed with depth	0.058	0.029	0.087	d^{-1}
b_D	Initial sinking speed	0.0	0.0	0.0	m d^{-1}

For all biogeochemical models considered here, the light intensity influences the biogeochemical processes, especially the biological production. The light limitation function $I : \Omega \times [0, 1] \rightarrow \mathbb{R}_{\geq 0}$ depends on the insolation computed on the fly using the astronomical formula of Paltridge and Platt (1976), and takes into account the ice cover as well as the exponential attenuation of water and (if included in the model) phytoplankton. Based on light intensity, the ocean Ω is divided into a euphotic (sun lit) zone of about 100 m and an aphotic zone below. The euphotic zone, in particular, exhibits a fast and dynamic turnover of phosphorus, for example through photosynthesis, grazing or mortality. One part of the biological production sinks as particulate matter from the euphotic zone to depth, where it is remineralized according to the empirical power law relationship discovered by Martin et al. (1987).

The simplest model of the hierarchy takes phosphate (PO_4) only as inorganic nutrient into account (Kriest et al., 2010). We denote this model as N model (N for nutrients) and $\mathbf{y} = (\mathbf{y}_N)$. The phytoplankton production

$$f_P : \Omega \times [0, 1] \rightarrow \mathbb{R}, f_P(x, t) = \mu_P y_P^* \frac{I(x, t)}{K_I + I(x, t)} \frac{\mathbf{y}_N(x, t)}{K_N + \mathbf{y}_N(x, t)} \quad (7)$$

depends on the light intensity and is limited by using a half saturation function, a maximum production rate parameter μ_P and a prescribed concentration of phytoplankton $y_P^* = 0.0028 \text{ mmol P m}^{-3}$. This model contains $n_u = 5$ model parameters $\mathbf{u} = (k_w, \mu_P, K_N, K_I, b)$ describing the internal processes, and resembles the model of Bacastow and Maier-Reimer (1990).

The second model of this hierarchy includes dissolved organic phosphorus (DOP) in addition to nutrients (N) (cf. Kriest et al., 2010; Bacastow and Maier-Reimer, 1991; Parekh et al., 2005). Hence, we denote this model as N-DOP model with the tracers $\mathbf{y} = (\mathbf{y}_N, \mathbf{y}_{\text{DOP}})$. The $n_u = 7$ model parameters $\mathbf{u} = (k_w, \mu_P, K_N, K_I, \sigma_{\text{DOP}}, \lambda'_{\text{DOP}}, b)$ control the internal processes using the unchanged phytoplankton production (7).

Resolving explicitly phytoplankton (P) increases the model complexity receiving the NP-DOP model, i.e., $\mathbf{y} = (\mathbf{y}_N, \mathbf{y}_P, \mathbf{y}_{\text{DOP}})$ (Kriest et al., 2010). Instead of using y_P^* in (7), the phytoplankton production (explicitly) includes the phytoplankton concentration \mathbf{y}_P . In addition, the phytoplankton concentration affects the light intensity. Moreover, the model contains a term for zooplankton grazing

$$f_Z : \Omega \times [0, 1] \rightarrow \mathbb{R}, f_Z(x, t) = \mu_Z y_Z^* \frac{\mathbf{y}_P(x, t)^2}{K_P^2 + \mathbf{y}_P(x, t)^2} \quad (8)$$

using the implicitly prespecified zooplankton concentration $y_Z^* = 0.01 \text{ mmol P m}^{-3}$. Overall, this model includes the $n_u = 13$ model parameters $\mathbf{u} = (k_w, k_c, \mu_P, \mu_Z, K_N, K_P, K_I, \sigma_{\text{DOP}}, \lambda_P, \kappa_P, \lambda'_P, \lambda'_{\text{DOP}}, b)$.

Adding zooplankton (Z) increases again the complexity. We denote this model as NPZ-DOP model with the tracers $\mathbf{y} = (\mathbf{y}_N, \mathbf{y}_P, \mathbf{y}_Z, \mathbf{y}_{\text{DOP}})$ (Kriest et al., 2010). While the phytoplankton production is the same as for the NP-DOP model, the zooplankton grazing (8) includes (explicitly) the zooplankton concentration \mathbf{y}_Z instead of using y_Z^* . The $n_u = 16$ model parameters are $\mathbf{u} = (k_w, k_c, \mu_P, \mu_Z, K_N, K_P, K_I, \sigma_Z, \sigma_{\text{DOP}}, \lambda_P, \lambda_Z, \kappa_Z, \lambda'_P, \lambda'_Z, \lambda'_{\text{DOP}}, b)$.

The last model of the hierarchy, the NPZD-DOP model, is similar to the model introduced by Schmittner et al. (2005) and explicitly resolves detritus (D), i.e., $\mathbf{y} = (\mathbf{y}_N, \mathbf{y}_P, \mathbf{y}_Z, \mathbf{y}_D, \mathbf{y}_{\text{DOP}})$. Both the phytoplankton production and the zooplankton grazing are unchanged. The model contains the model parameters $\mathbf{u} = (k_w, k_c, \mu_P, \mu_Z, K_N, K_P, K_I, \sigma_Z, \sigma_{\text{DOP}}, \lambda_P, \lambda_Z, \kappa_Z, \lambda'_P, \lambda'_Z, \lambda'_D, \lambda'_{\text{DOP}}, a_D, b_D)$, i.e., $n_u = 18$ (cf. Kriest et al., 2010).

In addition to the model hierarchy, we applied the model of Dutkiewicz et al. (2005) used for the MIT general circulation model biogeochemistry tutorial (cf. Marshall et al., 1997; Sokolov et al., 2005). This model includes phosphate (PO_4) and dissolved organic phosphorus (DOP) and resembles the N-DOP model. We denote this model as MITgcm- PO_4 -DOP model. The $n_u = 7$ model parameters are shown in Table 2 and correspond to the model parameters of the N-DOP model with different parameter names.

Table 2. Parameter values (\mathbf{u}_{ref}) used for the MITgcm-PO4-DOP model and the symbol used by Dutkiewicz et al. (2005) as well as lower (\mathbf{b}_ℓ) and upper (\mathbf{b}_u) bound for the parameter values used to generate the Latin hypercube sample.

Parameter	Description	\mathbf{u}_{ref}	\mathbf{b}_ℓ	\mathbf{b}_u	Unit
κ_{remin}	Decay rate	0.5	0.25	1.0	yr^{-1}
α	Maximum growth rate	2.0	1.0	4.0	mmol P m^{-3}
f_{DOP}	Fraction of phytoplankton losses assigned to DOP	0.67	0.05	0.095	1
κ_{PO_4}	Half saturation constant for PO_4 uptake	0.5	0.25	1.0	mmol P m^{-3}
κ_{I}	Light intensity compensation	30.0	15.0	60.0	W m^{-2}
k	Attenuation coefficient of water	0.02	0.01	0.05	m^{-1}
a_{remin}	Implicit representation of sinking speed	0.858	0.7	1.5	1

2.3 Transport matrix method

The transport matrix method (TMM) introduced by Khatiwala et al. (2005) is an efficient offline method for the simulation of tracer transports (cf. Khatiwala, 2007). For offline models, the ocean circulation takes the velocity field v and the diffusion fields κ_h, κ_v into account that can be pre-computed by some ocean circulation model running into a steady annual cycle. The TMM takes advantage of the fact that the application of the two operators D and A on a spatially discretized tracer vector is linear. Therefore, the discretized advection-diffusion equation can be written as a linear matrix equation. Hence, the TMM approximates the ocean circulation by matrices rather than to implement a discretization scheme for diffusion and advection. Instead of storing the fields v, κ_h and κ_v , the TMM computes and stores uniquely the matrices which represent the application of the discretized operators on a discrete tracer vector. This approach ensures that the matrices contain the transport of all parameterized processes represented in the ocean circulation model (Khatiwala et al., 2005).

The TMM reduces a time step of the marine ecosystem model to two matrix-vector-multiplications and one evaluation of the biogeochemical model. We assume that the grid with $n_x \in \mathbb{N}$ grid points $(x_k)_{k=1}^{n_x}$ is a spatial discretization of the domain Ω (i.e., the ocean) and the time steps $t_0, \dots, t_{n_t} \in [0, 1]$, $n_t \in \mathbb{N}$, specified by

$$t_j := j\Delta t, \quad j = 0, \dots, n_t, \quad \Delta t := \frac{1}{n_t},$$

define an equidistant grid of the time interval $[0, 1]$ (i.e., one model year). For the time instant t_j , $j \in \{0, \dots, n_t - 1\}$, the vector

$$\mathbf{y}_{ji} \approx (y_i(t_j, x_k))_{k=1}^{n_x} \in \mathbb{R}^{n_x}$$

contains the numerical approximation of the spatially discrete tracer y_i , $i \in \{1, \dots, n_y\}$, at the fixed time instant t_j and $\mathbf{y}_j := (\mathbf{y}_{ji})_{i=1}^{n_y} \in \mathbb{R}^{n_y n_x}$ includes the numerical approximation of all tracers at time instant t_j using a reasonable concatenation. Analogously,

$$\mathbf{q}_{ji} \approx (q_i(x_k, t_j, \mathbf{y}_j, \mathbf{u}))_{k=1}^{n_x} \in \mathbb{R}^{n_x}$$

denotes the spatially discretized biogeochemical term of tracer y_i , $i \in \{1, \dots, n_y\}$, at time instant t_j , $j \in \{0, \dots, n_t - 1\}$, and $\mathbf{q}_j := (\mathbf{q}_{ji})_{i=1}^{n_y}$ the spatially discretized biogeochemical term of all tracers at time instant t_j . Applying a semi-implicit Euler scheme, where the advection and the horizontal diffusion are discretized explicitly and the vertical diffusion implicitly, the discretization of (1) results in a time-stepping

$$\mathbf{y}_{j+1} = (\mathbf{I} + \Delta t \mathbf{A}_j + \Delta t \mathbf{D}_j^h) \mathbf{y}_j + \Delta t \mathbf{D}_j^v \mathbf{y}_{j+1} + \Delta t \mathbf{q}_j(\mathbf{y}_j, \mathbf{u}), \quad j = 0, \dots, n_t - 1$$

with the identity matrix $\mathbf{I} \in \mathbb{R}^{n_x \times n_x}$ and the spatially discretized counterparts \mathbf{A}_j , \mathbf{D}_j^h and \mathbf{D}_j^v of the operators A , D_h and D_v at time instant t_j , $j \in \{0, \dots, n_t - 1\}$. Defining the explicit and implicit transport matrices

$$\mathbf{T}_j^{\text{exp}} := \mathbf{I} + \Delta t \mathbf{A}_j + \Delta t \mathbf{D}_j^h \in \mathbb{R}^{n_x \times n_x},$$

$$\mathbf{T}_j^{\text{imp}} := (\mathbf{I} - \Delta t \mathbf{D}_j^v)^{-1} \in \mathbb{R}^{n_x \times n_x}$$

for each time instant t_j , $j \in \{0, \dots, n_t - 1\}$, a time step of the marine ecosystem model using the TMM is specified by

$$\mathbf{y}_{j+1} = \mathbf{T}_j^{\text{imp}} (\mathbf{T}_j^{\text{exp}} \mathbf{y}_j + \Delta t \mathbf{q}_j(\mathbf{y}_j, \mathbf{u})) =: \varphi_j(\mathbf{y}_j, \mathbf{u}), \quad j = 0, \dots, n_t - 1. \quad (9)$$

The transport matrices are sparse and represent the monthly averaged tracer transport respectively. Due to the calculation of the matrices with a grid-point based ocean circulation model, the explicit ones are sparse. Moreover, the implicit ones (i.e., the inverse of the discretization matrices) are sparse because they contain only the vertical part of the diffusion. Storing the transport matrices for all time-steps in a year is practically impossible. Therefore, monthly averaged matrices are stored. As a consequence, the matrices are interpolated linearly to compute an approximation for any time instant t_j , $j = 0, \dots, n_t - 1$. Assuming annual periodicity of the ocean circulation, twelve pairs of pre-computed transport matrices approximate the ocean circulation. Khatiwala et al. (2005) presented the details of the transport matrix computation.

We have used twelve explicit and twelve implicit transport matrices representing the monthly averaged tracer transport. These matrices are derived from the MIT ocean model (Marshall et al., 1997) using a global configuration with a latitudinal and longitudinal resolution of 2.8125° with 15 vertical layers.

2.4 Computation of steady annual cycles

For the marine ecosystem model, the steady annual cycle is a fixed-point of time integration over one model year. The steady annual cycle defined as a periodic solution of the system (1) to (6) with a period length of one model year fulfills

$$\mathbf{y}_{n_t} = \mathbf{y}_0$$

in the fully discrete setting applying the above iteration (9). The nonlinear mapping

$$\Phi := \varphi_{n_t-1} \circ \dots \circ \varphi_0$$

with φ_j defined in (9) corresponds to the time integration of (9) over one model year. In particular, a steady annual cycle is a fixed-point of the mapping Φ . Starting from an arbitrary vector $\mathbf{y}^0 \in \mathbb{R}^{n_y n_x}$, a classical fixed-point iteration takes the form

$$\mathbf{y}^{\ell+1} = \Phi(\mathbf{y}^\ell, \mathbf{u}), \quad \ell = 0, 1, \dots \quad (10)$$

The vector $\mathbf{y}^\ell := \mathbf{y}_{(\ell-1)n_t} \in \mathbb{R}^{n_y n_x}$ contains the tracer concentrations at the first time instant of model year $\ell \in \mathbb{N}$ if we interpret the fixed-point iteration as pseudo-time stepping or *spin-up*. If Φ is a contraction mapping fulfilling

$$\|\Phi(\mathbf{x}, \mathbf{u}) - \Phi(\mathbf{z}, \mathbf{u})\| \leq L \|\mathbf{x} - \mathbf{z}\|$$

for all $\mathbf{x}, \mathbf{z} \in \mathbb{R}^{n_y n_x}$ with $L \in [0, 1[$ in some norm, the Banach fixed-point theorem (cf. Banach, 1922; Dahmen and Reusken, 2008) ensures the convergence of the spin-up towards a unique fixed-point for all initial tracer concentrations $\mathbf{y}^0 \in \mathbb{R}^{n_y n_x}$. This result is also valid for weaker assumptions (cf. Ćirić, 1974). This approach of computing a fixed-point yields a robust method. However, the convergence behavior is only linear, and the estimation of $L = \max_{\mathbf{z} \in \mathbb{R}^{n_y n_x}} \|\Phi'(\mathbf{z}, \mathbf{u})\|$ is difficult due to the involved Jacobian $\mathbf{q}'_j(\mathbf{y}_j, \mathbf{u})$ of the nonlinear biogeochemical model for the current time instant t_j , $j \in \{0, \dots, n_t - 1\}$. In order to reach a steady annual cycle the spin-up ordinarily requires several thousand applications of the mapping Φ (i.e., model years) (cf. Bernsen et al., 2008). In order to test the numerical convergence of the iteration (10), we measured the periodicity of the steady annual cycle by the difference between two consecutive iterates defined by

$$\varepsilon_\ell := \|\mathbf{y}^\ell - \mathbf{y}^{\ell-1}\| \tag{11}$$

for iteration (i.e., model year) $\ell \in \mathbb{N}$.

2.5 Norms

We used various norms to quantify the difference between different tracer concentrations. For $\mathbf{z} \in \mathbb{R}^{n_y n_x}$ indexed as $\mathbf{z} = ((z_{ik})_{k=1}^{n_x})_{i=1}^{n_y}$ in accordance with the tracer indexing in Sect. 2.3, we defined a weighted Euclidean norm

$$\|\mathbf{z}\|_{2,w} := \left(\sum_{i=1}^{n_y} \sum_{k=1}^{n_x} w_k z_{ik}^2 \right)^{\frac{1}{2}}$$

with weights $w_k \in \mathbb{R}_{>0}$ for $k \in \{1, \dots, n_x\}$. A special case of this weighted Euclidean norm $\|\cdot\|_{2,w}$ is the Euclidean norm $\|\cdot\|_2$ if $w_k = 1$ holds for all $k \in \{1, \dots, n_x\}$. We introduced the norm $\|\cdot\|_{2,V}$ as a weighed Euclidean norm $\|\cdot\|_{2,w}$ with the weights $w_k = |V_k|$, $k \in \{1, \dots, n_x\}$, where $|V_k|$ denotes the box volume corresponding to the grid point x_k . This norm $\|\cdot\|_{2,V}$ is the discretized counterpart of the $(L^2(\Omega))^{n_y}$ norm. For all weight vectors $\mathbf{w} \in \mathbb{R}_{>0}^{n_x}$ and any vector $\mathbf{z} \in \mathbb{R}^{n_y n_x}$, particularly, holds

$$\min_{1 \leq k \leq n_x} \sqrt{w_k} \|\mathbf{z}\|_2 \leq \|\mathbf{z}\|_{2,w} \leq \max_{1 \leq k \leq n_x} \sqrt{w_k} \|\mathbf{z}\|_2,$$

i.e., the Euclidean norm $\|\cdot\|_2$ and the weighted Euclidean norm $\|\cdot\|_{2,w}$ are equivalent in the mathematical sense for all positive weights. Furthermore, we used a weighted Euclidean norm $\|\cdot\|_{2,w,T}$ for the whole trajectory of all tracers over one model year. For a vector $\mathbf{z} \in \mathbb{R}^{n_t n_y n_x}$ indexed as $\mathbf{z} = (((z_{jik})_{k=1}^{n_x})_{i=1}^{n_y})_{j=0}^{n_t-1}$ and a weight vector $\mathbf{w} \in \mathbb{R}_{>0}^{n_x}$, we defined the norm

$$\|\mathbf{z}\|_{2,w,T} := \left(\sum_{i=1}^{n_y} \sum_{j=0}^{n_t-1} \Delta t \sum_{k=1}^{n_x} w_k z_{jik}^2 \right)^{\frac{1}{2}}.$$

We denote in analogy to the weighted Euclidean norm by $\|\cdot\|_{2,T}$ the norm $\|\cdot\|_{2,w,T}$ with weights $w_k = 1$, $k \in \{1, \dots, n_x\}$, and by $\|\cdot\|_{2,V,T}$ the weighted Euclidean norm $\|\cdot\|_{2,w,T}$ where the weights are set to $w_k := |V_k|$, $k \in \{1, \dots, n_x\}$.

2.6 Influence of model to data misfit

We evaluated the steady annual cycle by measuring the difference between the calculated tracer concentrations and observations from the world ocean database (Boyer et al., 2013; Reimer, 2019). The approximation of the observations by the calculated steady annual cycles were comparable when using the following norm for different time steps. The norm is based on norm $\|\cdot\|_{2,T}$ taking into account only points in space and time for which there are observations available. Thereby, we applied only the quality controlled datasets. In order to take the number of measurements at the same point in space and time into account, we applied the world ocean database instead of the world ocean atlas (Garcia et al., 2014). There are available both points in space and time with many measurements and points for which there are no measurements. Hence, we skipped the discrete points in space and time without measurements in the norm. If many measurements exist at a discrete point in space and time, the norm, by contrast, involved each measurement individually.

We denoted by $n_{m_{ijk}} \in \mathbb{N}_0$ the number of measurements for the given tracer \mathbf{y}_i , $i \in \{1, \dots, n_y\}$, the point in time t_j , $j \in \{0, \dots, n_t - 1\}$ and the grid point x_k , $k \in \{1, \dots, n_x\}$. We combined all quality controlled datasets of the world ocean database in the vector $\mathbf{y}_{\text{data}} \in \mathbb{R}^{n_m}$ indexed as $\mathbf{y}_{\text{data}} = \left(\left(\left((y_{\text{data},j i k l})_{l=1}^{n_{m_{ijk}}} \right)_{k=1}^{n_x} \right)_{i=1}^{n_y} \right)_{j=0}^{n_t-1}$ with $n_m := \sum_{i=1}^{n_y} \sum_{j=0}^{n_t-1} \sum_{k=1}^{n_x} n_{m_{ijk}}$. We defined the discrete cost function of ordinary least squares (OLS) (Seber and Wild, 2003) as

$$J_{\text{OLS}}(\mathbf{z}) := \|\mathbf{z} - \mathbf{y}_{\text{data}}\|_{2,T,\text{OLS}}^2 := \sum_{i=1}^{n_y} \sum_{j=0}^{n_t-1} \sum_{k=1}^{n_x} \sum_{l=1}^{n_{m_{ijk}}} (z_{jik} - y_{\text{data},j i k l})^2 \quad (12)$$

for a vector $\mathbf{z} \in \mathbb{R}^{n_t n_y n_x}$ indexed as $\mathbf{z} = \left(\left((z_{jik})_{k=1}^{n_x} \right)_{i=1}^{n_y} \right)_{j=0}^{n_t-1}$.

3 Larger time steps

The increasing of the time step Δt leads to a shortening of the runtime of the spin-up. An increase of the time step reduces the computational effort because the spin-up needs several thousand model years to reach the steady annual cycle (cf. Bernsen et al., 2008). However, the dynamics in the ocean circulation limit the time step in marine ecosystem models to a few hours when the dynamical and tracer equations are integrated simultaneously (Khatiwala, 2007). Consequently, the computational effort is enormous for marine ecosystem models involving biogeochemical tracers to compute a steady annual cycle.

The transport matrices can be adjusted to the larger time step by simple matrix operations. When the transport matrices are generated, the time step of the underlying ocean circulation model directly enters each transport matrix. Nevertheless, Khatiwala (2007) described a possibility of the TMM to utilize larger time steps with minimal loss of accuracy. We generated transport matrices

$$\mathbf{T}_{j,m}^{\text{exp}} := \mathbf{I} + m(\mathbf{T}_j^{\text{exp}} - \mathbf{I}) \quad (13)$$

$$\mathbf{T}_{j,m}^{\text{imp}} := \left(\mathbf{T}_j^{\text{imp}} \right)^m \quad (14)$$

for every time instant t_j , $j \in \{0, \dots, n_t - 1\}$, whose effective time step is by a factor $m \in \mathbb{N}$ larger compared to the underlying ocean circulation model. The explicit transport matrix $\mathbf{T}_{j,m}^{\text{exp}}$ is, thereby, the exact representation of the rougher time step while

Table 3. Temporal resolution of the TMM using different time steps.

Time step	n_t	Corresponding time steps
1 dt	2880	3 h
2 dt	1440	6 h
4 dt	720	12 h
8 dt	360	24 h
16 dt	180	48 h
32 dt	90	96 h
64 dt	45	192 h

the implicit transport matrix $\mathbf{T}_{j,m}^{\text{imp}}$ is an approximation only which is asymptotically correct (Piwonski and Slawig, 2016b). The transport matrices for rougher time steps maintain even their sparsity (Khatiwala, 2007).

Assuming 360 days per year, the temporal resolution of the ocean circulation model used for the computation of the transport matrices $\mathbf{T}_j^{\text{exp}}, \mathbf{T}_j^{\text{imp}}, j \in \{0, \dots, n_t - 1\}$, corresponds to 3 h. Accordingly, the number of time steps per year is $n_t = 2880$. We identified this temporal resolution with time step 1 dt. Additionally, the transport matrices $\mathbf{T}_{j,1}^{\text{exp}}, \mathbf{T}_{j,1}^{\text{imp}}, j \in \{0, \dots, n_t - 1\}$, belong to this time step 1 dt.

We have studied the time steps listed in Table 3. Time step 2 dt conformed, for instance, to a doubling of the effective time step in (13) and (14). It is obvious that the use of larger time steps reduces the number of steps per year. In order to distinguish the tracer concentrations calculated with different time steps, we defined the vector $\mathbf{y}^{\ell,t}$ as the vector \mathbf{y}^ℓ computed with the time step t dt for $\ell \in \mathbb{N}_0$ and $t \in \{1, 2, 4, 8, 16, 32, 64\}$. More importantly, the transport matrices $\mathbf{T}_{j,t}^{\text{exp}}, \mathbf{T}_{j,t}^{\text{imp}}, j \in \{0, \dots, n_t - 1\}$, replace here the transport matrices $\mathbf{T}_j^{\text{exp}}, \mathbf{T}_j^{\text{imp}}$ in (9).

4 Results

In this section, we are presenting the results obtained for the biogeochemical models introduced in Sect. 2.2. We investigated the accuracy of the calculated steady annual cycles using larger time steps (cf. Sect. 3).

4.1 Experimental setup

For the computation of a steady annual cycle, we applied the marine ecosystem toolkit for optimization and simulation in 3D (Metos3D), a framework for the offline simulation of marine ecosystem models developed by Piwonski and Slawig (2016a, b). Here, we computed a spin-up of over 10000 model years starting with constant global mean tracer concentrations. Except for PO_4 , we initialized each tracer (i.e., the tracer DOP, P, Z and D) with a global mean tracer concentration of $0.0001 \text{ mmol P m}^{-3}$ in each simulation. PO_4 , i.e., the nutrient tracer N, was initialized with a global mean tracer concentration of $2.17 \text{ mmol P m}^{-3}$. We saved the tracer concentration of all the 50th model years during the spin-up.

Table 4. Relative error (15) with $\ell = 10000$ and $t \in \{2, 4, 8, 16, 32, 64\}$ for the whole model hierarchy.

Time step	N	N-DOP	NP-DOP	NPZ-DOP	NPZD-DOP
2 dt	7.816e-05	7.994e-05	4.715e-04	5.537e-04	5.757e-04
4 dt	2.239e-04	2.248e-04	1.277e-03	1.383e-03	1.398e-03
8 dt	5.022e-04	5.106e-04	2.912e-03	2.997e-03	2.795e-03
16 dt	1.084e-03	1.214e-03	6.212e-03	1.942e-02	1.722e-02
32 dt	2.259e-03	2.775e-03	1.355e-02	5.513e-02	6.146e-02
64 dt	4.035e-03	4.923e-03	-	-	-

We computed steady annual cycles for different parameter vectors. First, we are showing the results for the parameter vectors shown in Tables 1 and 2 for each biogeochemical model respectively. Next, we applied a Latin hypercube (cf. McKay et al., 1979) sample of 100 parameter vectors for all model parameters within the bounds of Table 1. We created these parameter vectors by the `lhs` routine of Lee (2014). We restricted the parameters of the created Latin hypercube sample to the required model parameters for each model (see Table 1). In order to use these Latin hypercube samples for the MITgcm-PO4-DOP model, we identified the restricted parameters $(\lambda'_{\text{DOP}}, \mu_P, \sigma_{\text{DOP}}, K_N, K_I, k_w, b)$ of the N-DOP model in this context with the parameters $(\kappa_{\text{remin}}, \alpha, f_{\text{DOP}}, \kappa_{\text{PO}_4}, \kappa_I, k, a_{\text{remin}})$ of the MITgcm-PO4-DOP model (see Table 2).

We compared the calculation of the steady annual cycle using a larger time step with a reference solution, namely the result obtained by a spin-up using Metos3D with time step 1 dt. For this comparison, we used several criteria, such as the norm (11), the cost function (12) and the required model years to reach a tolerance of 10^{-4} in (11) during the spin-up. We measured, in particular, the accuracy of the results of the spin-ups by the relative differences

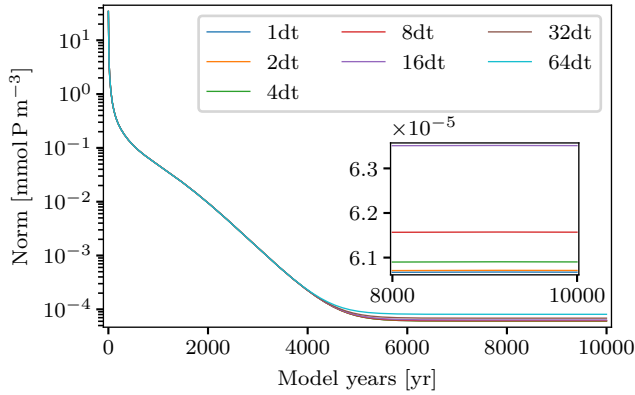
$$\frac{\|\mathbf{y}^{\ell,t} - \mathbf{y}^{10000,1}\|}{\|\mathbf{y}^{10000,1}\|} \quad \text{for } \ell \in \{50, 100, \dots, 10000\}, t \in \{2, 4, 8, 16, 32, 64\}, \quad (15)$$

$$\frac{|\mathbf{y}^{\ell,t} - \mathbf{y}^{10000,1}|}{\|\mathbf{y}^{10000,1}\|} \quad \text{for } \ell \in \{50, 100, \dots, 10000\}, t \in \{2, 4, 8, 16, 32, 64\}. \quad (16)$$

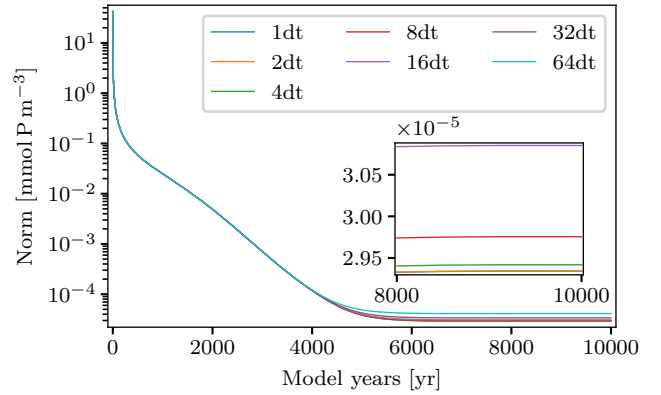
We call this quantity (15) the *(relative) error* of the respective result $\mathbf{y}^{\ell,t}$.

4.2 Larger time steps

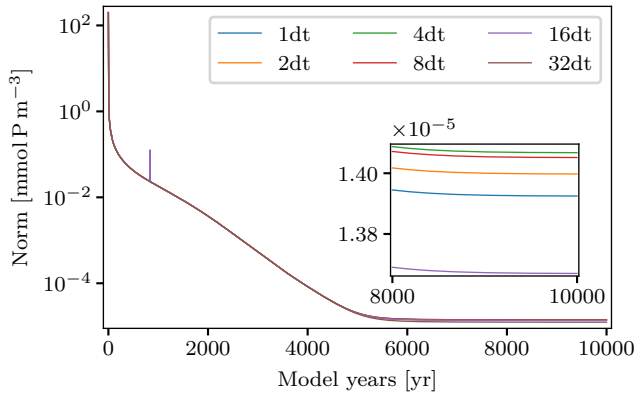
The spin-ups calculated with different time steps reflected the same steady annual cycle approximately. We first analyzed the influence of the time step on the accuracy of the steady annual cycle using one parameter vector for each biogeochemical model. We used the parameter vectors



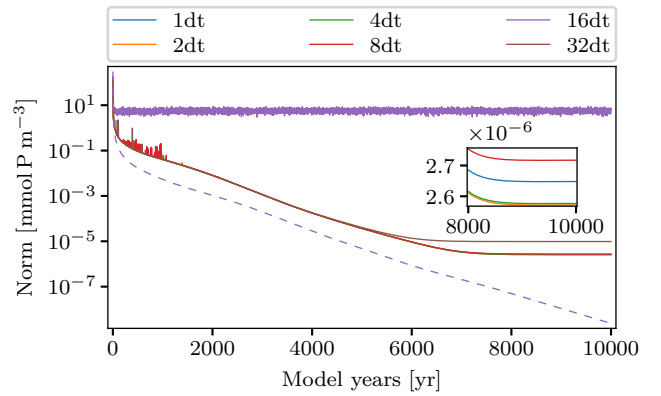
(a) N model using parameter vector \mathbf{u}_N (17).



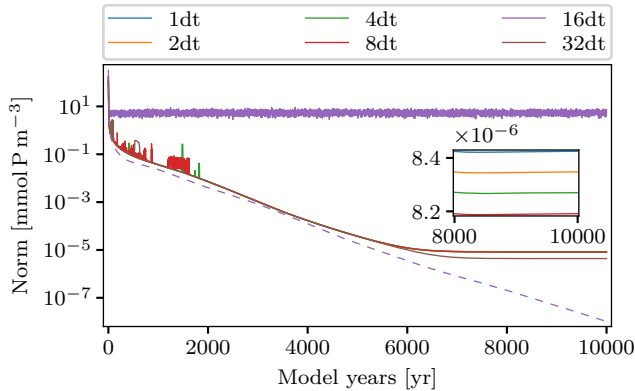
(b) N-DOP model using parameter vector \mathbf{u}_{N-DOP} (18).



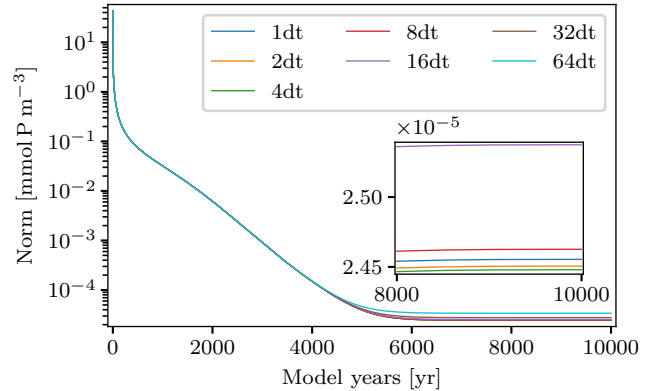
(c) NP-DOP model using parameter vector \mathbf{u}_{NP-DOP} (19).



(d) NPZ-DOP model using parameter vector $\mathbf{u}_{NPZ-DOP}$ (20).

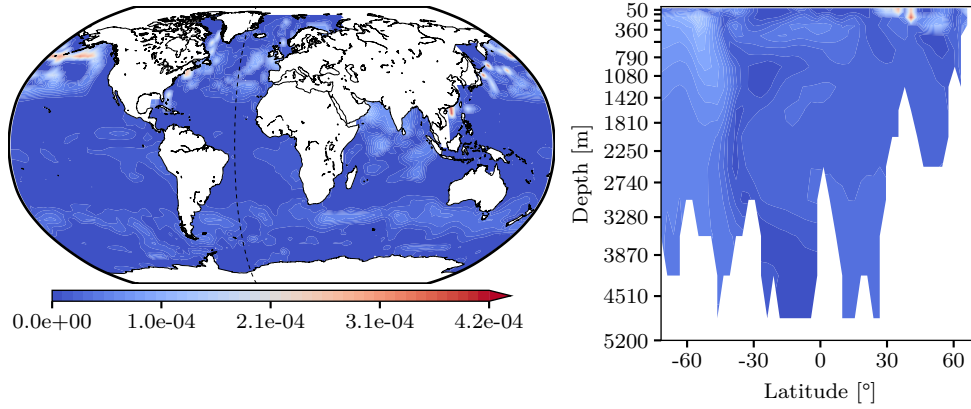


(e) NPZD-DOP model using parameter vector $\mathbf{u}_{NPZD-DOP}$ (21).

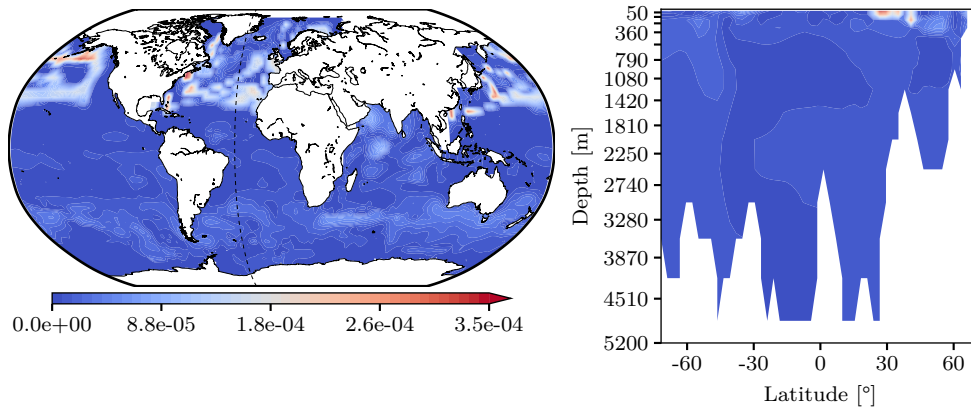


(f) MITgcm-PO4-DOP model using parameter vector \mathbf{u}_{ref} (22).

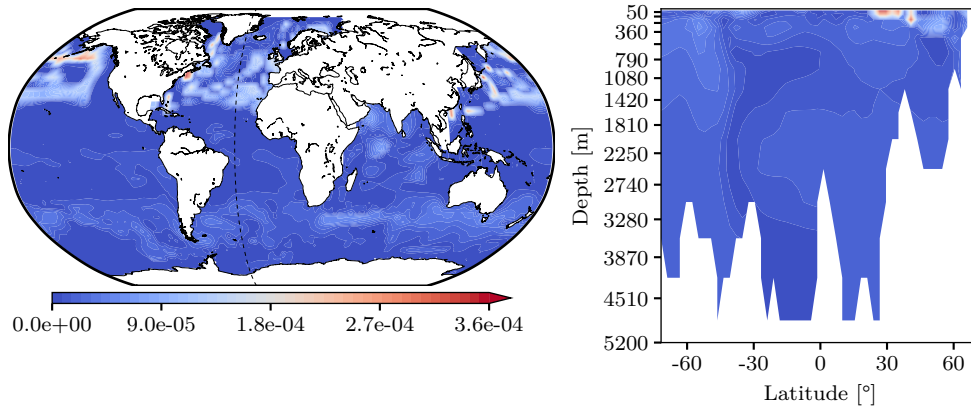
Figure 1. Norm of the difference (11) between two consecutive iterations in the spin-up for one parameter vector using different time steps (see Table 3). Additionally, the dashed line in Figs. 1d and 1e shows the norm of the differences (11) for the spin-up where all tracers were initialized with a global mean concentration of $0.542575 \text{ mmol P m}^{-3}$ (Fig. 1d) and $0.43408 \text{ mmol P m}^{-3}$ (Fig. 1e).



(a) N model using parameter vector \mathbf{u}_N (17).

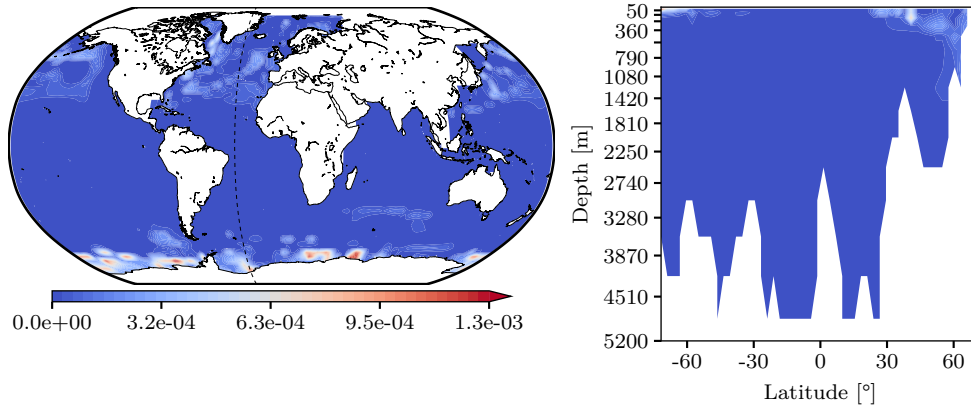


(b) N-DOP model using parameter vector \mathbf{u}_{N-DOP} (18).

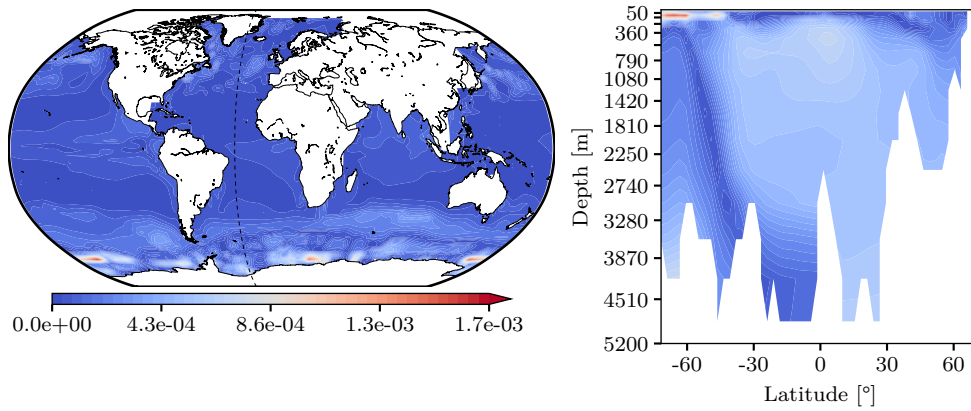


(c) MITgcm-PO4-DOP model using parameter vector \mathbf{u}_{ref} (22).

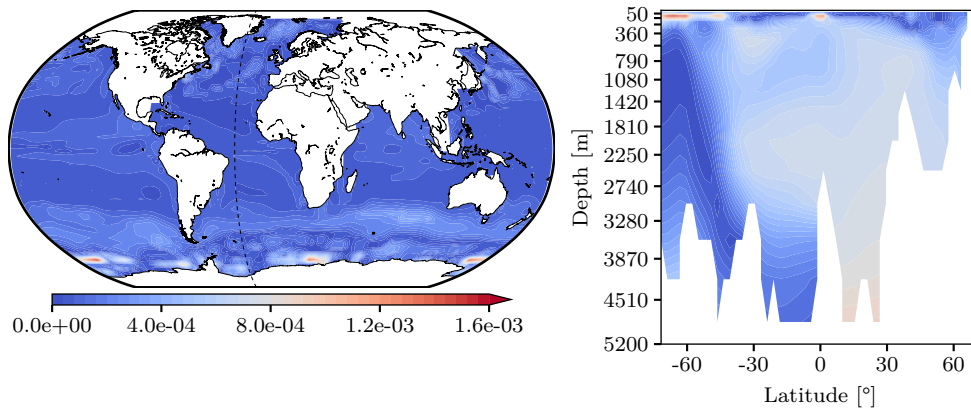
Figure 2. Relative error (16) with $\ell = 10000$ and $t = 64$ of the phosphate concentrations at the surface layer (0 m to 50 m, left) and at a slice plane of the Atlantic at 29.53125° W (located at the dashed line, right) at the first time instant of the model year (in January).



(a) NP-DOP model using parameter vector $\mathbf{u}_{\text{NP-DOP}}$ (19).

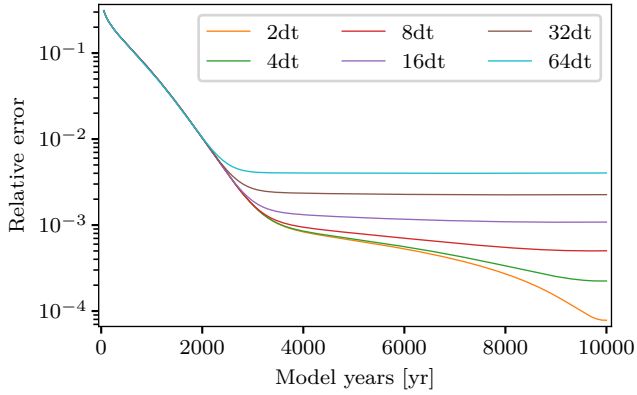


(b) NPZ-DOP model using parameter vector $\mathbf{u}_{\text{NPZ-DOP}}$ (20).

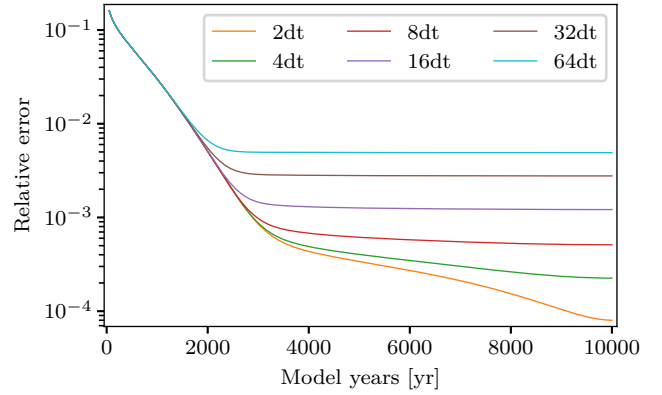


(c) NPZD-DOP model using parameter vector $\mathbf{u}_{\text{NPZD-DOP}}$ (21).

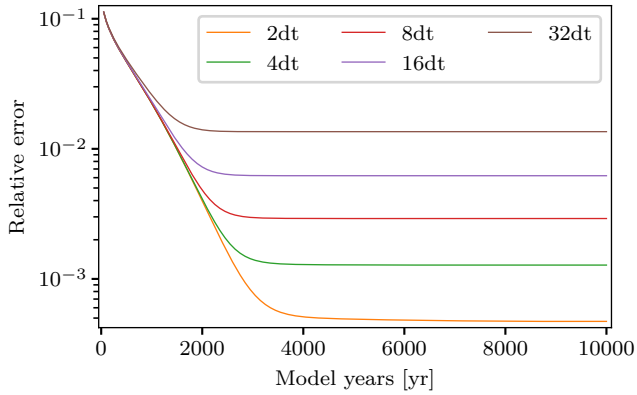
Figure 3. As Fig. 2, but for $t = 32$ and the other biogeochemical models.



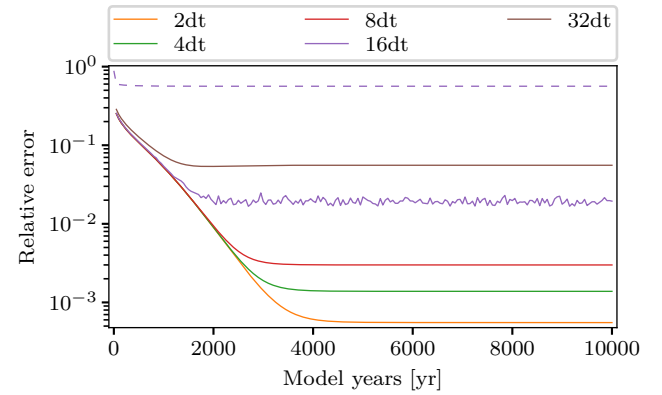
(a) N model using parameter vector \mathbf{u}_N (17).



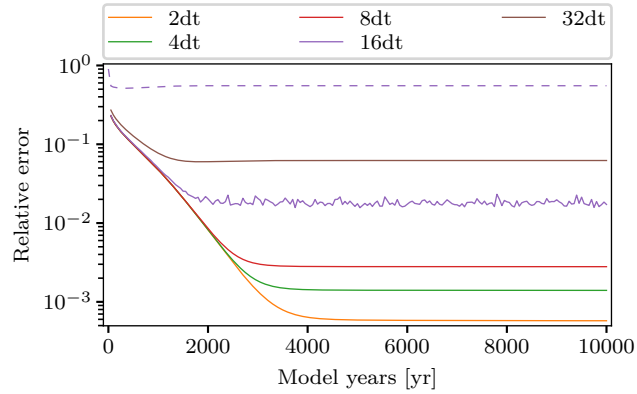
(b) N-DOP model using parameter vector \mathbf{u}_{N-DOP} (18).



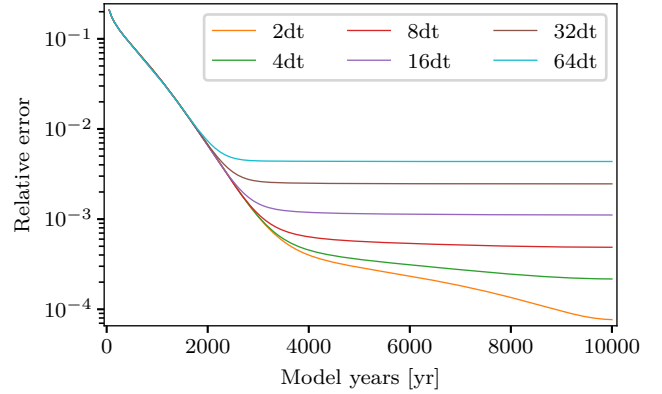
(c) NP-DOP model using parameter vector \mathbf{u}_{NP-DOP} (19).



(d) NPZ-DOP model using parameter vector $\mathbf{u}_{NPZ-DOP}$ (20).



(e) NPZD-DOP model using parameter vector $\mathbf{u}_{NPZD-DOP}$ (21).



(f) MITgcm-PO4-DOP model using parameter vector \mathbf{u}_{ref} (22).

Figure 4. Relative error (15) in the Euclidean norm of the spin-up using different time steps for $\ell \in \{50, 100, \dots, 10000\}$, $t \in \{2, 4, 8, 16, 32, 64\}$ and one parameter vector respectively. The dashed line represents the relative error calculated with a global mean concentration of $0.542575 \text{ mmol P m}^{-3}$ (Fig. 4d) and $0.43408 \text{ mmol P m}^{-3}$ (Fig. 4e) for each tracer.

$$\mathbf{u}_N = (0.02, 2.0, 0.5, 30.0, 0.858) \quad (17)$$

$$\mathbf{u}_{N-DOP} = (0.02, 2.0, 0.5, 30.0, 0.67, 0.5, 0.858) \quad (18)$$

$$\mathbf{u}_{NP-DOP} = (0.02, 0.48, 2.0, 2.0, 0.5, 0.088, 30.0, 0.67, 0.04, 4.0, 0.01, 0.5, 0.858) \quad (19)$$

$$\mathbf{u}_{NPZ-DOP} = (0.02, 0.48, 2.0, 2.0, 0.5, 0.088, 30.0, 0.75, 0.67, 0.04, 0.03, 3.2, 0.01, 0.01, 0.5, 0.858) \quad (20)$$

$$\mathbf{u}_{NPZD-DOP} = (0.02, 0.48, 2.0, 2.0, 0.5, 0.088, 30.0, 0.75, 0.67, 0.04, 0.03, 3.2, 0.01, 0.01, 0.05, 0.5, 0.058, 0.0) \quad (21)$$

$$\mathbf{u}_{ref} = (0.5, 2.0, 0.67, 0.5, 30.0, 0.02, 0.858) \quad (22)$$

(see Tables 1 and 2). Figure 1 demonstrates a similar convergence behavior for all different time steps whereas the spin-up reached nearly the same accuracy for the norm of differences (11). For the NP-DOP, NPZ-DOP and NPZD-DOP model, the spin-up calculation using time step 64 dt was aborted due to a technical error as consequence of a too large step size of the Euler method. Moreover, the norm of differences oscillated and the spin-up did not converge when using time step 16 dt for the NPZ-DOP and NPZD-DOP model. For all biogeochemical models, the magnitude of the error (16) increased when larger time steps were used (for the models N, N-DOP and MITgcm-PO4-DOP from 10^{-6} (2 dt) to 10^{-3} (64 dt) and the same also for the models NP-DOP, NPZ-DOP and NPZD-DOP from 10^{-5} (2 dt) to 10^{-3} (32 dt)) (Figs. 2 and 3). With each model, the largest errors occurred almost in the same regions for the different time steps. Likewise, this was observed with the other tracers. More specifically, the accuracy of the calculated steady annual cycles decreased not only on the surface layer but also in the entire ocean when larger time steps were used as shown in Fig. 4 and Table 4. Namely, the accuracy developed equally for all time steps for the first model years but the error reduction stagnated earlier with increasing time steps during the spin-up. Although the norm of the differences (11) oscillated and did not converge using time step 16 dt for the NPZ-DOP and NPZD-DOP model (Figs. 1d and 1e), the relative error was between those calculated with time steps 8 dt and 32 dt. The choice of the norm (i.e., volume-weighted norm $\|\cdot\|_{2,V}$ or comparing the whole trajectory $\|\cdot\|_{2,V,T}$) did not lead to any qualitative difference in the calculation of the relative error (15) (Table 5). The cost function values in Table 6 indicate that the steady annual cycle when calculated with larger time steps reflected the data of the world ocean database in a similar manner as the steady annual cycle calculated with time step 1 dt. However, the cost function values were quite large for all models and time steps because the parameter vectors have not been optimized for the steady state to reflect the data optimally.

The reason for the divergence of the solution using time step 64 dt was the too large step size for the Euler method. The biogeochemical model, for example, used more nutrients than available in a box of the spatial discretization for one time step and converted these into particle like plankton due to the large time step. Thus, the concentration in this box became negative, i.e., the model ran empty. As a consequence, the model produced mass because the biogeochemical model set the negative concentration value to zero but did not subtract the absolute value anywhere else. On the contrary, the biogeochemical model did not generate negative concentrations because the equations of this model are quasi-positive (cf. Pierre, 2010), and the transport matrix method also does not generate negative concentrations. Indeed, the negative concentrations occurred due to the too large step size of the Euler method and, subsequently, caused the increase of absolute value of the negative concentrations and, as a result, of the positive concentrations during the spin-up. Therefore, NaN (not a number) arose in the computation of

Table 5. The use of different norms for the relative error (15) with $\ell = 10000$ and $t \in \{2, 4, 8, 16, 32, 64\}$ for the MITgcm-PO4-DOP model and parameter vector \mathbf{u}_{ref} (22).

Time step	$\ \cdot\ _2$	$\ \cdot\ _{2,V}$	$\ \cdot\ _{2,V,T}$
2 dt	7.680e-05	4.007e-05	7.008e-05
4 dt	2.168e-04	1.158e-04	2.845e-04
8 dt	4.872e-04	2.594e-04	8.741e-04
16 dt	1.111e-03	5.587e-04	2.377e-03
32 dt	2.462e-03	1.166e-03	6.032e-03
64 dt	4.360e-03	2.061e-03	1.497e-02

Table 6. Cost function values of type ordinary least squares (12) for the whole model hierarchy. Shown are the cost functions values $J_{\text{OLS}}(\mathbf{y}^{10000,t})$ of the spin-up using the exemplary parameter vectors (cf. Tables 1 and 2) for $t \in \{1, 2, 4, 8, 16, 32, 64\}$, respectively. For the calculation of the cost function, only the N tracer was used because hardly any measurement data are available for the other tracers.

Time step	N	N-DOP	NP-DOP	NPZ-DOP	NPZD-DOP	MITgcm-PO4-DOP
1 dt	1.093e+06	9.834e+05	1.261e+06	1.274e+06	1.232e+06	8.375e+05
2 dt	1.110e+06	9.930e+05	1.268e+06	1.280e+06	1.235e+06	8.473e+05
4 dt	2.428e+06	1.471e+06	1.558e+06	1.805e+06	1.551e+06	1.297e+06
8 dt	2.927e+06	1.626e+06	1.665e+06	1.999e+06	1.673e+06	1.456e+06
16 dt	1.657e+06	1.315e+06	1.507e+06	1.590e+06	1.499e+06	1.223e+06
32 dt	1.686e+06	1.402e+06	1.609e+06	1.626e+06	1.480e+06	1.292e+06
64 dt	1.713e+06	1.490e+06	-	-	-	1.366e+06

the quadratic loss term for phytoplankton in the zooplankton grazing (8) due to the large phytoplankton concentration which became infinite in the quadratic term of the numerator as well as that of the denominator.

The oscillation of the difference norm (11) resulted from an inappropriate step size of the Euler method (Figs. 1d and 1e). For the spin-up calculation with 16 dt, the oscillation occurred for each tracer. The oscillation started on the ocean surface and spread to deeper layers during the spin-up so that the oscillation appeared in the lowest layer between 4510 m to 5200 m only after 2000 model years. The magnitude of the norm of differences, and consequently of the oscillation, decreased on deeper layers because the annual concentration change on deeper layers is marginal. Apart from that, the occurrence of oscillations depended on the initial tracer concentrations (Figs. 1d and 1e, dashed line). For the changed initial concentration, the spin-up, however, ended with an invalid steady annual cycle (Figs. 4d and 4e, dashed line) because, first, all tracers had nearly constant concentrations, second, all the mass was concentrated in the N tracer, and third, the other tracers (P, Z and DOP) had negative concentrations exclusively. This was a consequence of a too large time step for the Euler method.

Table 7. Count of parameter sets of the Latin hypercube sample without spin-up convergence after 10000 model years for different time steps.

Time step	N	N-DOP	NP-DOP	NPZ-DOP	NPZD-DOP	MITgcm-PO4-DOP
1 dt	0	0	0	0	0	0
2 dt	0	0	0	0	0	0
4 dt	0	0	0	0	0	0
8 dt	0	0	0	0	0	0
16 dt	0	0	0	0	0	0
32 dt	0	0	0	5	3	0
64 dt	0	0	45	47	46	0

Table 8. Count of parameter sets of the Latin hypercube sample with oscillations of the norm of differences (11) during the spin-up.

Time step	N	N-DOP	NP-DOP	NPZ-DOP	NPZD-DOP	MITgcm-PO4-DOP
1 dt	0	0	5	12	14	0
2 dt	0	0	4	13	14	0
4 dt	0	0	6	27	23	0
8 dt	0	0	8	43	34	0
16 dt	0	0	8	60	62	0
32 dt	0	0	45	36	46	0
64 dt	0	0	27	19	35	0

In short, all steady annual cycles calculated with larger time steps practically approximated the reference solution for the whole model hierarchy. The accordance between the reference solution and the steady annual cycle computed with larger time steps decreased slowly with larger time steps, on the one hand, and, on the other hand, slightly with the complexity of the biogeochemical model as detailed in Table 4.

4.3 Parameter samples

In this section, we analyzed the behavior for the different time steps utilizing the parameter vectors of the Latin hypercube sample for all biogeochemical models. In the previous Sect. 4.2, we discussed this behavior exclusively for one (reference) parameter vector for each model.

The accuracy of the approximation of the steady annual cycle decreased with larger time steps. For the three biogeochemical models N, N-DOP and MITgcm-PO4-DOP, the spin-up calculations almost always converged with a norm of differences (11) less than 10^{-4} whereby the difference increased only slightly for larger time steps (Figs. 5a, 5b and 5f). In contrast, the spin-ups for the other three models NP-DOP, NPZ-DOP and NPZD-DOP ended up with a much larger norm of differences

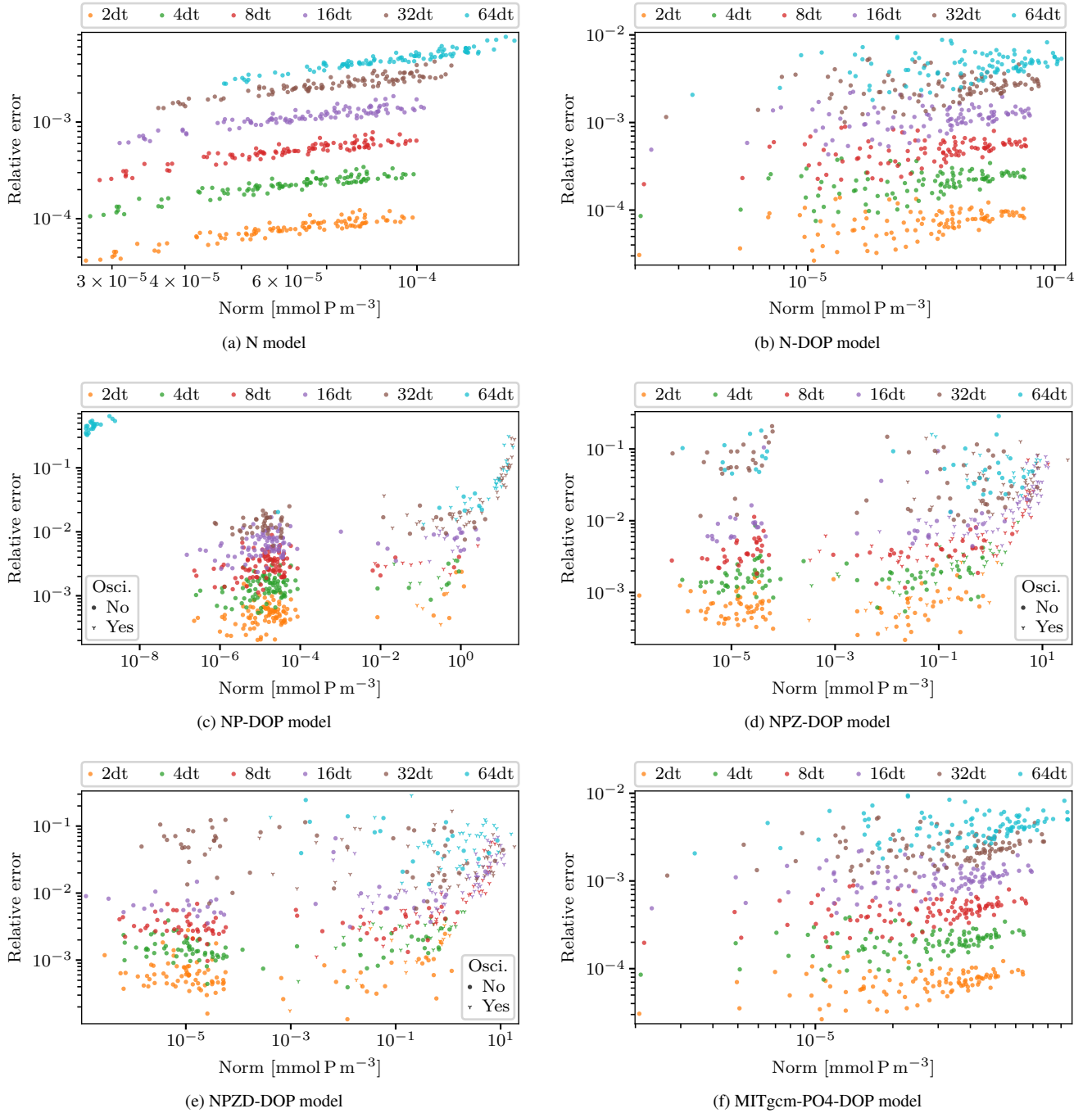


Figure 5. Visualization of the norm of the differences (11) and the relative error (15) in the Euclidean norm for $\ell = 10000$ using different time steps for all parameter vectors of the Latin hypercube sample.

Table 9. Count of parameter sets of the Latin hypercube sample, which reached a spin-up tolerance of less than 10^{-4} mmol P m⁻³ after 10000 model years, for the whole model hierarchy and different time steps.

Time step	N	N-DOP	NP-DOP	NPZ-DOP	NPZD-DOP	MITgcm-PO4-DOP
1 dt	100	100	90	51	64	100
2 dt	100	100	89	52	64	100
4 dt	100	100	86	40	54	100
8 dt	100	100	86	32	45	100
16 dt	98	100	77	19	22	100
32 dt	89	100	42	23	26	100
64 dt	61	96	24	12	0	100

between two successive iterations (11) for numerous parameter vectors (Figs. 5c, 5d and 5e). As a result of a too large time step, the spin-up calculation diverged for almost 50% of the parameter vectors when using time step 64 dt (Table 7). For one half of these parameter vectors, the spin-up did not converge for all three models. For the parameter vectors of the other half, either the spin-up diverged exclusively for the NP-DOP model or did not converge for the NPZ-DOP and NPZD-DOP model. Furthermore, the spin-up using time step 64 dt was always divergent if the spin-up calculation diverged using time step 32 dt for the same model and parameter vector. In addition, oscillations of the norm of differences (11) occurred frequently when time steps larger than 4 dt for these three models were used as detailed in Table 8. There were parameter vectors for which oscillations occurred for exactly one time step as well as parameter vectors for which oscillations appeared for several (up to even all) time steps. The values of the individual model parameter of the parameter vectors covered the entire range in each case so that the oscillations could not be traced back to the value of an individual model parameter. Nonetheless, Fig. 5 shows the approximately identical magnitude of the relative error (15) for each time step, regardless of both the norm of differences (11) and the occurrence of oscillations. Analogously to the results for the reference parameter vector (see Sect. 4.2), the relative error increased, on the one hand, with larger time steps and, on the other hand, with the complexity of the biogeochemical model. Moreover, the steady annual cycles matched the data of the world ocean database in a similar way for all time steps. As for the reference parameters (see Table 6), the cost function values (12) calculated with time step 1 dt nearly corresponded to those calculated with 2 dt whereas the values calculated with larger time steps were slightly higher.

The use of larger time steps significantly reduced the computational effort with practically the same approximation of the steady annual cycle. Except for a few outliers, the number of model years to obtain a tolerance of 10^{-4} in (11) was nearly identical for the different time steps (Fig. 6). Both with the complexity of the biogeochemical model and with the size of the time step, the number of parameter vectors increased for which the spin-up did not reach the tolerance of 10^{-4} after a maximum of 10000 model years (Table 9). If the spin-up did not reach the desired spin-up tolerance for a time step, the spin-up using a larger time step in most cases did not reach this spin-up tolerance either for the same parameter vector. Nevertheless, there were parameter vectors accomplishing the desired spin-up tolerance for larger time steps in contrast to smaller time steps. Not

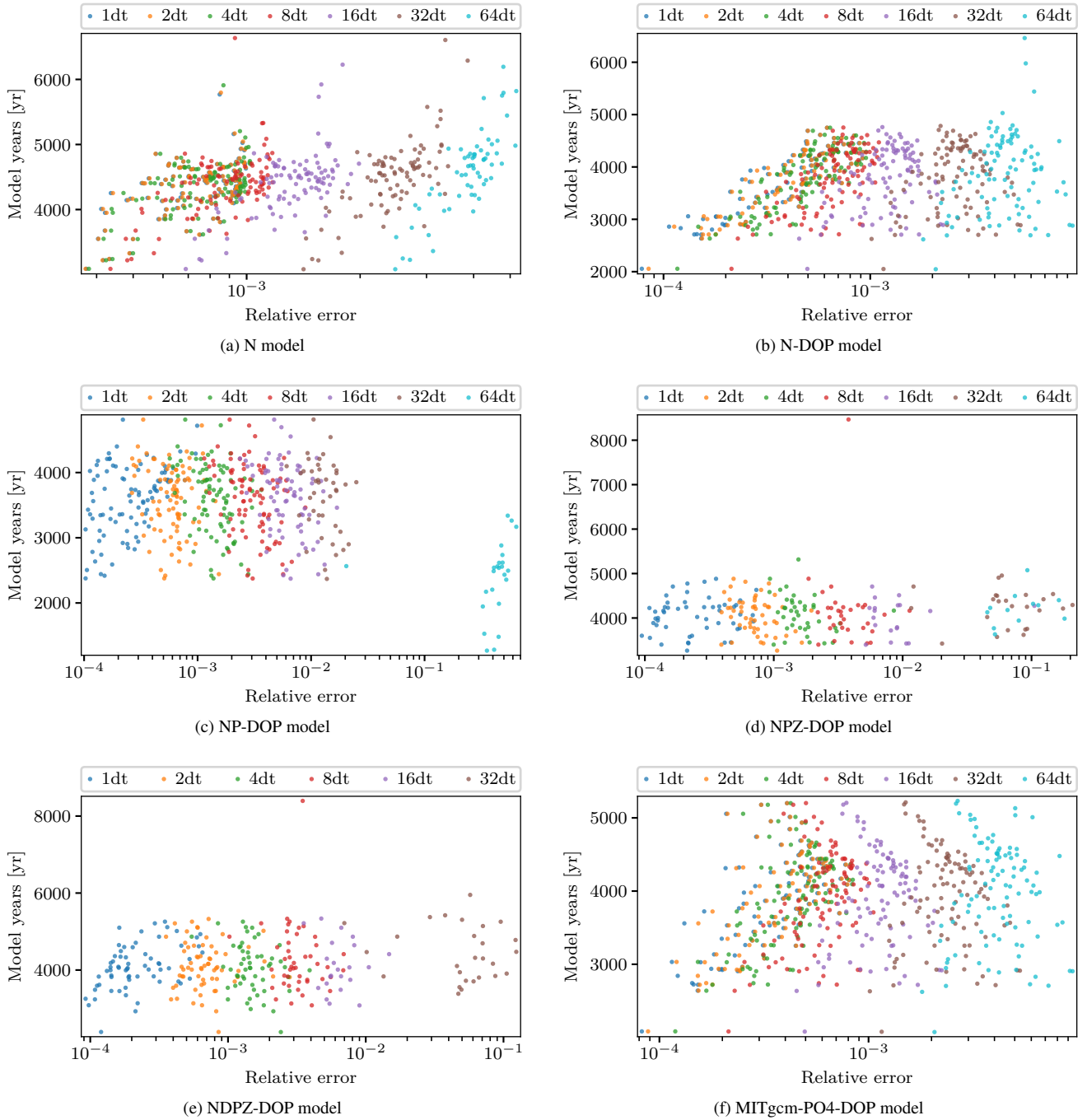


Figure 6. Required model years for reaching a tolerance 10^{-4} in (11) in the spin-up and relative error (15) of the corresponding model year using different time steps for all parameter vectors of the Latin hypercube sample.

any parameter vector, for example, existed for which the spin-up reached the tolerance of 10^{-4} using the NPZD-DOP model. Figure 6 indicates that the tracer concentrations, calculated with a spin-up using time steps smaller than 8 dt, approximated the steady state in the same way for the N, N-DOP and MITgcm-PO4-DOP model while the relative error continuously increased when time steps larger than 8 dt were used. Conversely, the deviation from the steady annual cycle of the reference solution grew steadily when larger time steps were used for the other three models NP-DOP, NPZ-DOP and NPZD-DOP. In particular, the deviations using time step 64 dt (for all three models) as well as 32 dt (for the NPZ-DOP and NPZD-DOP model) were noticeable.

5 Conclusions

Using larger time steps to compute steady annual cycles provided practically the same solution for marine ecosystem models based on the TMM, and shortened the runtime. We computed steady annual cycles for a hierarchy of biogeochemical models of increasing complexity (cf. Kriest et al., 2010; Dutkiewicz et al., 2005) using larger time steps to reduce the computational effort. Apart from that, the solution computed with a larger time step conformed with the solution calculated with time step 1 dt with a suitable precision. More importantly, we can mostly apply larger time steps to compute steady annual cycles with a decreased computational effort.

The error between the reference solution and the solution calculated with a larger time step increased with larger time steps. This occurred by reason of the discretization error of the explicit Euler method (Stoer and Bulirsch, 2002) and of the utilization of an approximation of the transport matrix for larger time steps (Khatiwala, 2007; Piwonski and Slawig, 2016b). The aim was to determine the time step as large as possible so that the discretization error is small enough. For the three most complex models, for example, the relative error exceeded 10^{-2} using time steps larger as 8 dt (cf. Figs. 4 and 5). Hence, the time step must be selected for every model so that the error is appropriate for the particular application of the steady annual cycle. However, the accuracy of norm of differences (11) did not allow to suggest the accuracy of the solution.

The divergence of the spin-up using larger time steps for the three biogeochemical models with the highest complexity, we have explained by a too large step size for the Euler method. As a consequence, the biogeochemical model ran empty because the model required, for example, more nutrients than were available in a box of the discretization due to the large time step. As a result, the concentration became negative. The absolute value of the concentrations increased during the spin-up so that NaN arose by the computation of the zooplankton grazing because the numerator as well as the denominator of the quadratic term became infinite (cf. (8)). Subsequently, the occurrence of NaN increased because the result of an operation is NaN if at least one operand is NaN (Goldberg, 1991). The divergence depended, additionally, on the model complexity and the parameters.

The application of larger time steps lowered the computational costs of the steady annual cycle calculation for marine ecosystem models. Instead of 2880 time steps per model year using time step 1 dt, time step 2 dt merely takes up 1440 time steps per model year and time step 64 dt only requires 45 time steps per model year. Therefore, a speed-up factor of up to 64 is possible when larger time steps are used. The TMM easily supports the application of larger time steps (Khatiwala, 2007) and Piwonski and Slawig (2016b) implemented this application in Metos3D. Our results provide crucial evidence that

the application of larger time steps practically yielded the same solution. For instance, Prieß et al. (2013) applied time step 64 dt using Metos3D and Kriest and Oschlies (2015) as well as Kriest et al. (2017) used time step 4 dt with the TMM for the computation of steady annual cycles, respectively.

We have computed the steady annual cycle based on the application of larger time steps for many different parameter sets in a huge domain for each one of the models of the model hierarchy. The model assessment (e.g., Kriest et al., 2010), the model calibration (e.g., Kriest, 2017) or the sensitivity analysis (e.g., Kriest et al., 2012) of global marine biogeochemical models requires quite a lot of computations of a steady annual cycle. Hence, using larger time steps lowers the computational cost considerably. Another field of application for the use of larger time steps is the parameter identification (for example carried out in Prieß et al., 2013). Accordingly, the runtime can considerably be shortened using larger time steps because the optimization needs the computation of a steady annual cycle for several parameter sets. Future work will be directed to implement an algorithm for the computation of a steady annual cycle using automatically the largest possible time step, such as a step size control.

In summary, the main points are the following:

- Using larger time steps shortened the runtime of simulations of marine ecosystem models.
- The computation of a steady annual cycle using larger time steps for marine ecosystem models practically yielded the same solution.
- A too large time step led to a divergent spin-up calculation, especially for complex biogeochemical models.

Code and data availability. The code used to generate the data in this publication is available at <https://github.com/slavig/bgc-ann>, <https://metos3d.github.io/> and <https://github.com/jor-/simulation>. We applied version v0.5.0 of Metos3D - with version v0.2.2 of the Metos3D data package, v0.3.3 of the Metos3D model package and v0.5.0 of the Metos3D simulation package - for all numerical experiments. All used and generated data are available at <https://doi.org/10.5281/zenodo.5643706> (Pfeil and Slawig, 2021).

References

- Bacastow, R. B. and Maier-Reimer, E.: Ocean-circulation model of the carbon cycle, *Climate Dynamics*, 4, 95–125, <https://doi.org/10.1007/BF00208905>, 1990.
- Bacastow, R. B. and Maier-Reimer, E.: Dissolved organic carbon in modeling oceanic new production, *Global Biogeochemical Cycles*, 5, 71–85, <https://doi.org/10.1029/91GB00015>, 1991.
- Banach, S.: Sur les opérations dans les ensembles abstraits et leur application aux équations intégrales, *Fundamenta Mathematicae*, 3, 133–181, <http://eudml.org/doc/213289>, 1922.
- Bernsen, E., Dijkstra, H. A., and Wubs, F. W.: A method to reduce the spin-up time of ocean models, *Ocean Modelling*, 20, 380 – 392, <https://doi.org/10.1016/j.ocemod.2007.10.008>, 2008.
- Boyer, T. P., Antonov, J. I., Baranova, O. K., Coleman, C., Garcia, H. E., Grodsky, A., Johnson, D. R., Locarnini, R. A., Mishonov, A. V., O'Brien, T. D., Paver, C. R., Reagan, J. R., Seidov, D., Smolyar, I. V., and Zweng, M. M.: World Ocean Database 2013, Tech. rep., NOAA Atlas NESDIS 72, Silver Spring, s. Levitus, Ed.; A. Mishonov, Technical Ed., 2013.
- Bryan, K.: Accelerating the Convergence to Equilibrium of Ocean-Climate Models, *Journal of Physical Oceanography*, 14, 666–673, [https://doi.org/10.1175/1520-0485\(1984\)014<0666:ATCTEO>2.0.CO;2](https://doi.org/10.1175/1520-0485(1984)014<0666:ATCTEO>2.0.CO;2), 1984.
- Ćirić, L. B.: A Generalization of Banach's Contraction Principle, *Proceedings of the American Mathematical Society*, 45, 267–273, <https://doi.org/10.2307/2040075>, 1974.
- Dahmen, W. and Reusken, A.: Numerik für Ingenieure und Naturwissenschaftler, Springer Lehrbuch, Springer-Verlag Berlin Heidelberg, 2 edn., <https://doi.org/10.1007/978-3-540-76493-9>, 2008.
- Danabasoglu, G., McWilliams, J. C., and Large, W. G.: Approach to Equilibrium in Accelerated Global Oceanic Models, *Journal of Climate*, 9, 1092–1110, [https://doi.org/10.1175/1520-0442\(1996\)009<1092:ATEIAG>2.0.CO;2](https://doi.org/10.1175/1520-0442(1996)009<1092:ATEIAG>2.0.CO;2), 1996.
- Dutkiewicz, S., Sokolov, A. P., Scott, J., and Stone, P. H.: A three-dimensional ocean-seaice-carbon cycle model and its coupling to a two-dimensional atmospheric model: Uses in climate change studies, Tech. Rep. 122, MIT Joint Program on the Science and Policy of Global Change, Cambridge, 2005.
- Fasham, M. J. R., ed.: Ocean Biogeochemistry, Global Change – The IGBP Series, Springer, Berlin et al., <https://doi.org/10.1007/978-3-642-55844-3>, 2003.
- Fennel, K., Losch, M., Schröter, J., and Wenzel, M.: Testing a marine ecosystem model: sensitivity analysis and parameter optimization, *Journal of Marine Systems*, 28, 45 – 63, [https://doi.org/10.1016/S0924-7963\(00\)00083-X](https://doi.org/10.1016/S0924-7963(00)00083-X), 2001.
- Fennel, W. and Neumann, T.: Introduction to the Modelling of Marine Ecosystems, vol. 72 of *Elsevier Oceanography Series*, Elsevier, 2004.
- Garcia, H. E., Locarnini, R. A., Boyer, T. P., Antonov, J. I., Baranova, O. K., Zweng, M. M., Reagan, J. R., and Johnson, D. R.: World Ocean Atlas 2013, Volume 4: Dissolved Inorganic Nutrients (phosphate, nitrate, silicate), Tech. rep., s. Levitus, Ed., A. Mishonov Technical Ed.; NOAA Atlas NESDIS 76, 25 pp., 2014.
- Goldberg, D.: What Every Computer Scientist Should Know About Floating-point Arithmetic, *ACM Computing Surveys*, 23, 5–48, <https://doi.org/10.1145/103162.103163>, 1991.
- Ilyina, T., Six, K. D., Segschneider, J., Maier-Reimer, E., Li, H., and Núñez-Riboni, I.: Global ocean biogeochemistry model HAMOCC: Model architecture and performance as component of the MPI-Earth system model in different CMIP5 experimental realizations, *Journal of Advances in Modeling Earth Systems*, 5, 287–315, <https://doi.org/10.1029/2012MS000178>, 2013.

- Keller, D. P., Oschlies, A., and Eby, M.: A new marine ecosystem model for the University of Victoria Earth System Climate Model, *Geoscientific Model Development*, 5, 1195–1220, <https://doi.org/10.5194/gmd-5-1195-2012>, 2012.
- Khatiwala, S.: A computational framework for simulation of biogeochemical tracers in the ocean, *Global Biogeochemical Cycles*, 21, <https://doi.org/10.1029/2007GB002923>, 2007.
- Khatiwala, S.: Fast spin up of Ocean biogeochemical models using matrix-free Newton-Krylov, *Ocean Modelling*, 23, 121–129, <https://doi.org/10.1016/j.ocemod.2008.05.002>, 2008.
- Khatiwala, S., Visbeck, M., and Cane, M. A.: Accelerated simulation of passive tracers in ocean circulation models, *Ocean Modelling*, 9, 51–69, <https://doi.org/10.1016/j.ocemod.2004.04.002>, 2005.
- Kriest, I.: Calibration of a simple and a complex model of global marine biogeochemistry, *Biogeosciences*, 14, 4965–4984, <https://doi.org/10.5194/bg-14-4965-2017>, 2017.
- Kriest, I. and Oschlies, A.: MOPS-1.0: towards a model for the regulation of the global oceanic nitrogen budget by marine biogeochemical processes, *Geoscientific Model Development*, 8, 2929–2957, <https://doi.org/10.5194/gmd-8-2929-2015>, 2015.
- Kriest, I., Khatiwala, S., and Oschlies, A.: Towards an assessment of simple global marine biogeochemical models of different complexity, *Progress In Oceanography*, 86, 337–360, <https://doi.org/10.1016/j.pocean.2010.05.002>, 2010.
- Kriest, I., Oschlies, A., and Khatiwala, S.: Sensitivity analysis of simple global marine biogeochemical models, *Global Biogeochemical Cycles*, 26, <https://doi.org/10.1029/2011GB004072>, gB2029, 2012.
- Kriest, I., Sauerland, V., Khatiwala, S., Srivastav, A., and Oschlies, A.: Calibrating a global three-dimensional biogeochemical ocean model (MOPS-1.0), *Geoscientific Model Development*, 10, 127–154, <https://doi.org/10.5194/gmd-10-127-2017>, 2017.
- Kwon, E. Y. and Primeau, F.: Optimization and sensitivity study of a biogeochemistry ocean model using an implicit solver and in situ phosphate data, *Global Biogeochemical Cycles*, 20, <https://doi.org/10.1029/2005GB002631>, 2006.
- Kwon, E. Y. and Primeau, F.: Optimization and sensitivity of a global biogeochemistry ocean model using combined in situ DIC, alkalinity, and phosphate data, *Journal of Geophysical Research: Oceans*, 113, <https://doi.org/10.1029/2007JC004520>, 2008.
- Le Quééré, C., Buitenhuis, E. T., Moriarty, R., Alvain, S., Aumont, O., Bopp, L., Chollet, S., Enright, C., Franklin, D. J., Geider, R. J., Harrison, S. P., Hirst, A. G., Larsen, S., Legendre, L., Platt, T., Prentice, I. C., Rivkin, R. B., Saille, S., Sathyendranath, S., Stephens, N., Vogt, M., and Vallina, S. M.: Role of zooplankton dynamics for Southern Ocean phytoplankton biomass and global biogeochemical cycles, *Biogeosciences*, 13, 4111–4133, <https://doi.org/10.5194/bg-13-4111-2016>, 2016.
- Lee, A.: pyDOE: Design of Experiments for Python, available at: <https://pythonhosted.org/pyDOE/index.html> (last access: November 17, 2021), 2014.
- Lotka, A. J.: Contribution to the Theory of Periodic Reactions, *The Journal of Physical Chemistry*, 14, 271–274, <https://doi.org/10.1021/j150111a004>, 1910.
- Marshall, J., Adcroft, A., Hill, C., Perelman, L., and Heisey, C.: A finite-volume, incompressible Navier Stokes model for studies of the ocean on parallel computers, *Journal of Geophysical Research: Oceans*, 102, 5753–5766, <https://doi.org/10.1029/96JC02775>, 1997.
- Martin, J. H., Knauer, G. A., Karl, D. M., and Broenkow, W. W.: VERTEX: carbon cycling in the northeast Pacific, *Deep Sea Research Part A. Oceanographic Research Papers*, 34, 267 – 285, [https://doi.org/10.1016/0198-0149\(87\)90086-0](https://doi.org/10.1016/0198-0149(87)90086-0), 1987.
- McKay, M. D., Beckman, R. J., and Conover, W. J.: A Comparison of Three Methods for Selecting Values of Input Variables in the Analysis of Output from a Computer Code, *Technometrics*, 21, 239–245, <https://doi.org/10.2307/1268522>, 1979.
- Oschlies, A.: Feedbacks of biotically induced radiative heating on upper-ocean heat budget, circulation, and biological production in a coupled ecosystem-circulation model, *Journal of Geophysical Research: Oceans*, 109, <https://doi.org/10.1029/2004JC002430>, 2004.

- Oschlies, A.: On the use of data assimilation in biogeochemical modelling, in: *Ocean Weather Forecasting*, edited by Chassignet, E. P. and Verron, J., pp. 525–547, Springer, Dordrecht, https://doi.org/10.1007/1-4020-4028-8_24, 2006.
- Paltridge, G. W. and Platt, C. M. R.: *Radiative Processes in Meteorology and Climatology*, Elsevier, New York, <https://doi.org/10.1002/qj.49710343713>, 1976.
- Parekh, P., Follows, M. J., and Boyle, E. A.: Decoupling of iron and phosphate in the global ocean, *Global Biogeochemical Cycles*, 19, <https://doi.org/10.1029/2004GB002280>, 2005.
- Pfeil, M. and Slawig, T.: Shortening the runtime using larger time steps for the simulation of marine ecosystem models, Zenodo [data set], <https://doi.org/10.5281/zenodo.5643706>, 2021.
- Pierre, M.: Global Existence in Reaction-Diffusion Systems with Control of Mass: a Survey, *Milan Journal of Mathematics*, 78, 417–455, <https://doi.org/10.1007/s00032-010-0133-4>, 2010.
- Piwonski, J. and Slawig, T.: Metos3D: the Marine Ecosystem Toolkit for Optimization and Simulation in 3-D – Part 1: Simulation Package v0.3.2, *Geoscientific Model Development*, 9, 3729–3750, <https://doi.org/10.5194/gmd-9-3729-2016>, 2016a.
- Piwonski, J. and Slawig, T.: Temporal Coarsening of Transport Matrices with Metos3D, Tech. Rep. 1608, Department of Computer Science, Kiel University, http://www.uni-kiel.de/journals/receive/jportal_jparticle_00000291, 2016b.
- Prieß, M., Piwonski, J., Koziel, S., Oschlies, A., and Slawig, T.: Accelerated parameter identification in a 3D marine biogeochemical model using surrogate-based optimization, *Ocean Modelling*, 68, 22–36, <https://doi.org/http://dx.doi.org/10.1016/j.ocemod.2013.04.003>, 2013.
- Reimer, J.: Statistical Analysis of the Phosphate Data of the World Ocean Database 2013, Preprint on arXiv, <https://arxiv.org/abs/1912.07384>, 2019.
- Sarmiento, J. L. and Gruber, N.: *Ocean biogeochemical dynamics*, Princeton University Press, Princeton et al., 2006.
- Schmittner, A., Oschlies, A., Giraud, X., Eby, M., and Simmons, H. L.: A global model of the marine ecosystem for long-term simulations: Sensitivity to ocean mixing, buoyancy forcing, particle sinking, and dissolved organic matter cycling, *Global Biogeochemical Cycles*, 19, <https://doi.org/10.1029/2004GB002283>, 2005.
- Seber, G. A. F. and Wild, C. J.: *Nonlinear Regression*, Wiley Series in Probability and Statistics, Wiley-Interscience, 2003.
- Siewertsen, E., Piwonski, J., and Slawig, T.: Porting marine ecosystem model spin-up using transport matrices to GPUs, *Geoscientific Model Development*, 6, 17–28, <https://doi.org/10.5194/gmd-6-17-2013>, 2013.
- Sokolov, A. P., Schlosser, C. A., Dutkiewicz, S., Paltsev, S., Kicklighter, D. W., Jacoby, H. D., Prinn, R. G., Forest, C. E., Reilly, J., Wang, C., Felzer, B. S., Sarofim, M. C., Scott, J. R., Stone, P. H., Melillo, J. M., and Cohen, J. B.: MIT Integrated Global System Model (IGSM) Version 2: Model Description and Baseline Evaluation, Tech. Rep. 124, MIT - Massachusetts Institute of Technology, 2005.
- Stoer, J. and Bulirsch, R.: Introduction to numerical analysis, vol. 12 of *Texts in applied mathematics*, Springer, New York, 3 edn., <https://doi.org/10.1007/978-0-387-21738-3>, 2002.
- Volterra, V.: Variations and fluctuations of the number of individuals in animal species living together, in: *Animal Ecology*, edited by Chapman, R. N., pp. 409–448, McGraw–Hill, New York, 1931.
- Wang, D.: A note on using the accelerated convergence method in climate models, *Tellus A: Dynamic Meteorology and Oceanography*, 53, 27–34, <https://doi.org/10.3402/tellusa.v53i1.12179>, 2001.
- Yool, A., Popova, E. E., and Anderson, T. R.: MEDUSA-2.0: an intermediate complexity biogeochemical model of the marine carbon cycle for climate change and ocean acidification studies, *Geoscientific Model Development*, 6, 1767–1811, <https://doi.org/10.5194/gmd-6-1767-2013>, 2013.